Title

Hierarchically Ordered Porous and High-Volume Polycaprolactone Microchannel Scaffolds Enhanced Axon Growth in Transected Spinal Cords.

Journal

Tissue engineering. Part A, 23(9-10)

ISSN

1937-3341

Authors

Shahriari, Dena
Koffler, Jacob Y
Tuszynski, Mark H
et al.

Publication Date

2017-05-01

DOI

10.1089/ten.tea.2016.0378

Peer reviewed

TISSUE ENGINEERING: Part A
Volume 23, Numbers 9 and 10, 2017

DOI: 10.1089/ten.tea.2016.0378

termis
Tissue Engineering
& Regenerative Medicine
International Society

ORIGINAL ARTICLE

Hierarchically Ordered Porous and High-Volume Polycaprolactone Microchannel Scaffolds Enhanced Axon Growth in Transected Spinal Cords

Dena Shahriari, PhD,[1] Jacob Y. Koffler, PhD,[2] Mark H. Tuszynski, MD, PhD,[2,3] Wendy M. Campana, PhD,[4,5] and Jeff S. Sakamoto, PhD[1,6]

The goal of this work was to design nerve guidance scaffolds with a unique architecture to maximize the open volume available for nerve growth. Polycaprolactone (PCL) was selected as the scaffold material based on its biocompatibility and month-long degradation. Yet, dense PCL does not exhibit suitable properties such as porosity, stiffness, strength, and cell adhesion to function as an effective nerve guidance scaffold. To address these shortcomings, PCL was processed using a modified salt-leaching technique to create uniquely controlled interconnected porosity. By controlling porosity, we demonstrated that the elastic modulus could be controlled between 2.09 and 182.1 MPa. In addition, introducing porosity and/or coating with fibronectin enhanced the PCL cell attachment properties. To produce PCL scaffolds with maximized open volume, porous PCL microtubes were fabricated and translated into scaffolds with 60 volume percent open volume. The scaffolds were tested in transected rat spinal cords. Linear axon growth within both the microtubes as well as the interstitial space between the tubes was observed, demonstrating that the entire open volume of the scaffold was available for nerve growth. Overall, a novel scaffold architecture and fabrication technique are presented. The scaffolds exhibit significantly higher volume than state-of-the-art scaffolds for promising spinal cord nerve repair.

Keywords: controlled porosity, mechanical properties, nerve guidance scaffolds, nerve regeneration, polycaprolactone

Introduction

There are no effective therapies to promote nerve repair after acute or chronic spinal cord injury (SCI) in adult humans.[1,2] Although recent progress has been made using interventional treatments, no approach has yet provided functional recovery. For example, various cellular (astrocytes, Schwann cells, or stem cells) approaches promote axon growth in SCI animal models to support axon attachment and elongation, but functional repair is yet to be reported.[3–6] An alternative approach to regenerate spinal cord axons is to provide physical cues to guide regenerating cells within the lesion site. Examples include electrospun fibers[7–10] and conduits.[11–14] While linear guidance of axons toward distal targets was demonstrated using several of these approaches, the ability to achieve native axon densities and functional spinal cord repair requires further technological and materials refinement. One approach toward achieving this goal is to utilize synthetic multichanneled nerve scaffolds that effectively guide axons along the damaged spinal cord.[11,15–21] Currently, microchannel scaffolds that are effective in linearly guiding axon growth within a SCI lesion have an open volume below 45%.[11,15–20] However, functional nerve repair may be achieved if a higher open volume is produced. Thus, there is a need to develop new materials and materials processing technology to enable the fabrication of biocompatible scaffolds.

To significantly improve open volume, rather than creating microchannels inside a material, we introduced a novel scaffold design utilizing the open space provided by channels that also allows axon growth between the channels. Our approach was to create scaffolds consisting of microtubes with thin walls assembled inside an outer tube that matched

[1]Department of Macromolecular Science and Engineering, University of Michigan, Ann Arbor, Michigan.
[2]Department of Neuroscience, University of California San Diego, La Jolla, California.
[3]Veterans Administration Medical Center, La Jolla, California.
[4]Department of Anesthesiology, University of California San Diego, La Jolla, California.
[5]Program in Neuroscience, University of California San Diego, La Jolla, California.
[6]Department of Mechanical Engineering, University of Michigan, Ann Arbor, Michigan.

the nerve fiber diameter. We also aimed to control porosity in the scaffold walls by creating <20 μm interconnected porosity. Such porosity allowed substrate permeation as well as optimizing stiffness and cell attachment properties.

Based on its strength and reported biocompatibility with the nerve tissue,[11,22,23] we chose polycaprolactone (PCL). PCL was also selected as a representative synthetic polymer based on its superior strength compared with hydrogels.[24–26] In its dense form, however, the stiffness and cell attachment properties may not be suitable for use in nerve guidance scaffolds.[26–28] The elastic moduli of dense PCL and the spinal cord are 300 MPa[29] and 0.68–3.5 Pa,[30,31] respectively. Thus, to better match the elastic modulus of the spinal cord, porosity was introduced into PCL.

There are several methods to introduce porosity into PCL such as photo crosslinking of a chemically modified PCL,[7,27] solvent casting,[24,29,32–36] and a customized patterning technique.[7,23] We chose a modified salt-leaching process, commonly used in ceramic material processing (high-energy planetary ball-milling [PMB]) that reduces porogen (NaCl) particle size to unprecedented length scales. This resulted in fewer micrometer-scale interconnected porosity and a porogen-induced secondary set of porosity. Changes in PCL porosity affected cell attachment. Fibroblasts robustly adhered to porous PCL without provisional extracellular matrix (fibronectin), whereas primary Schwann cell attachment required a fibronectin matrix. The modified PCL salt-leaching process was integrated into a fabrication process to produce microtubes (60 μm wall thickness and 260 μm inner diameter [ID]), whereby the walls consisted of interconnected pores. The microtubes were assembled into packed arrays to achieve >60 volume percent (vol %) open volume scaffolds.

Porous PCL scaffolds were implanted into rats with thoracic level 3 (T3) complete transections of the spinal cord to assess biocompatibility and ability to provide axonal guidance. Results herein show that porosity-modified PCL scaffolds with high volume had adequate strength to withstand fabrication and implantation, and were durable enough to maintain integrity for 4 weeks *in vivo*. Favorable integration with host tissue and linear axonal growth were observed. This study is the first report to generate interconnected few micrometer scale porosity in PCL using salt-leaching for scaffolds that support linear axon growth in SCI. The novel scaffold architecture introduced here has significantly higher open volume compared with previously reported microchannel nerve scaffolds (60% compared with 45% open volume) and is considered promising for advancing the field of spinal cord repair after traumatic nerve injuries.

Materials and Methods

Porogen size reduction

Sodium chloride (NaCl) was purchased from Columbus Chemical Industries, Inc. (Columbus, WI). NaCl (5 g) was placed in a 250 mL agate vial with twelve 9.1-mm diameter agate balls. A planetary ball-mill (Retsch PM 100, Haan, Germany) was used to reduce the NaCl particle size (Supplementary Fig. S1a, step 1; Supplementary Data are available online at www.liebertpub.com/tea). To study the effects of ball-milling time and vial rotational speeds on the particle size distribution, 100 and 400 revolutions per minute (rpm), and ball-milling times of 1, 5, 10, 30, 60, and 90 min were used. An alternating sequence of 5 min of ball-milling followed by 5 min rest was used to minimize media heating. In addition, the rotational direction was reversed after each 5 min rest to reduce NaCl particle agglomeration. The ball-milled NaCl particle morphology and size were characterized and measured using scanning electron microscopy (SEM; FEI Nova NanoLab™ 600 DualBeam, Columbus, OH). Owing to favorable particle size distributions, the NaCl ball-milled at 400 rpm for 60 min was used for all the polymer fabrication processes, unless is otherwise mentioned.

PCL/NaCl mixture preparation

ε-Caprolactone (molecular weight [MW]: 114.14; Sigma, St. Louis, MO) was dissolved in chloroform (3 weight percent) and mixed with 0–70 vol % of the NaCl ball-milled at 400 rpm for 60 min. The mixture (20–30 g) was ball-milled for 20 min at 400 rpm with 5 min rests every 5 min to enhance the dispersion of the NaCl (Supplementary Fig. S1a, step 2). The vol % of the NaCl in the PCL mixture corresponded to the intended vol % of porosity after solvent evaporation and salt-leaching.

PCL film fabrication and characterization

PCL films consisting of 0–70 vol % porosity were fabricated for mechanical testing and SEM imaging. To fabricate films, the ball-milled PCL/NaCl mixtures using NaCL ball-milled for 60 min at 400 rpm were cast using an automated tape casting coater (Supplementary Fig. S1b) (MTI Corporation, Richmond, CA). Copper foil (McMaster, Aurora, OH) was placed on the tape casting coater and the slurry was poured on the foil. A doctor blade (set at 50 μm clearance between the copper foil and bottom of the blade) was passed over the slurry, spreading it uniformly at 50 μm/s. The film was air dried after casting. To delaminate the PCL films from the copper foil, the films were moistened with methanol (Sigma). The NaCl was removed from the PCL films by placing the films in 2 L of tap water for 18 h.

To characterize the porosity of the films, PCL films were fractured in liquid nitrogen before and after salt-leaching, gold sputtered for 120 s and their cross-sectional images were taken using SEM. Films with 100% PCL remained ductile in liquid nitrogen and could not be fractured for SEM cross-sectional imaging. Therefore, the 100% PCL films were mounted in epoxy (Leco Corporation, St. Joseph, MI) and polished using 600, 1200, and 1500 grit sandpaper (McMaster). The cross-section was further polished with 12 and 6 μm diamond paste (Leco Corporation). The 100% PCL film was then coated with gold for SEM analysis.

To perform uniaxial tensile testing, films were cut to rectangular pieces of about 30 × 8 mm using a razor blade. A uniaxial tension test was performed on the films (Instron, Norwood, MA) under a constant extension rate of 0.2 mm/min.

Cell adhesion studies

PCL films (100% and 30 vol % porosity) were fabricated as described in PCL Film Fabrication and Characterization section and cut to the diameter of the wells of a tissue culture-treated 24-well plate, sterilized in ethanol, washed

three times with sterile phosphate-buffered saline (PBS), and placed under ultraviolet light for 30 min. Three different PCL materials were studied: (1) control substrate (tissue culture plate for fibroblasts and poly-D-lysine for Schwann cells—0.01 mg/mL coated directly on the tissue culture plate); (2) 100% PCL film; and (3) 30 vol % porous PCL film with and without fibronectin (1 mg/mL).

Primary rat Schwann cells or NIH 3T3 fibroblasts were plated at a seeding density of 5×10^4 cells/well. Fibroblasts were cultured in Dulbecco's modified Eagle's medium (DMEM; No. 11965; Thermo Fisher Scientific, Grand Island, NY) with 10% fetal bovine serum (FBS; No. 160000036; Thermo Fisher Scientific) and 1% Penicillin–Streptomycin–Glutamine (No. 10378016; Thermo Fisher Scientific). Primary rat Schwann cells were cultured in DMEM (No. 11885; Thermo Fisher Scientific) with 10% FBS, 1% Penicillin–Streptomycin (No. 15140122; Thermo Fisher Scientific), 21 μg/mL Bovine Pituitary Extract (BPE; CC-4009; Lonza, Allendale, NJ), and 4 μM Forskolin (No. 344270; Calbiochem, San Diego, CA). After 72 h, cells were washed twice with warm PBS and fixed with 4% formaldehyde for 10 min. PCL films were washed with PBS and blocked in 1% bovine serum albumin (BSA)/PBS for 20 min at room temperature. Alexa Fluor® phalloidin conjugates (Thermo Fisher Scientific) were used to identify cellular F-actin. The nuclei of the cells were stained with DAPI (Life Technologies, Carlsbad, CA) for 20 min and subsequently washed in PBS. Fluorescent images were taken (fluorescent microscope—Olympus BX53, Center Valley, PA).

Scaffold fabrication

PCL scaffolds were fabricated with 70 vol % porosity. The tube and scaffold fabrication process is illustrated in Figure 1a and b, respectively. A copper wire (99% purity; McMaster) with a diameter of 200 μm and a stainless steel rod (grade 304; McMaster) with a diameter of 1.60 mm were used to fabricate inner and outer tubes, respectively. The metal wires and rods (referred here as fibers) were placed in a PCL:NaCl mixture with 30:70 vol % and were removed after 5 s of immersion and spun manually while holding horizontally to uniformly evaporate the solvent. To facilitate delamination, the PCL-coated metal rods were immersed in methanol for about 30 s. The tubes were removed, dried in a fume hood, and cut into 2-mm-long tubes using a razor blade.

To fabricate scaffolds, 11 inner tubes (260 μm ID, 2 mm long) were inserted into an outer tube (1.6 mm ID, 2 mm long). Optical microscopy (Leica EZ4D, Buffalo Grove, IL) was used to image the scaffolds. The scaffold open volume percentage was calculated according to the following equation:

$$Scaffold\ open\ Volume = \frac{Outer\ Tube\ Open\ Volume - Volume\ of\ Innertube\ walls}{Outer\ Tube\ Open\ Volume} \times 100$$

The scaffolds were placed in water for at least 18 h to remove the NaCl and were sterilized in 5% ethanol in reverse osmosis water for 1 h. The scaffolds were coated with fibronectin (1 mg/mL) for 1 h and rinsed before implantation.

Surgical procedures

Adult female Fischer 344 rats (150–200 g) were housed 2–3 per cage with free access to food and water in a vivarium approved by the American Association for the Accreditation of Laboratory Animal Care. All animal studies were carried out according to protocols approved by the Institutional Animal Care and Use Committee of the VA Hospital (San Diego, CA) and following the IASP Guidelines for Use of Animals in Research.

Three experimental groups were studied: Sham surgeries ($n = 3$), transected spinal cords without implant ($n = 3$), and transected spinal cords receiving fibronectin-coated porous PCL scaffolds ($n = 8$). An incision was made in the skin of the back over the T2 spinous process. After clearing of the muscle, the dorsal aspect of the T3 vertebra was removed. Sham surgeries consisted of T3 laminectomy only. For other subjects, a longitudinal incision was made in the dura with a No. 11 blade, leaving the surface of the cord exposed. Small iridectomy scissors were used to bilaterally transect the cord at two sites in the center of the T3 spinal segment located 1.2 mm apart for animals receiving no implants and 2 mm apart for other animals, and the segment between the cuts was removed by aspiration. For $n = 3$ of the animals, no implants were inserted. Sterilized 70 vol % porosity PCL scaffolds coated with 1 mg/mL fibronectin (described in Scaffold Fabrication section) were surgically placed in the transected spinal cord. The muscles overlying the spinal cord were sutured and the skin incision was closed with

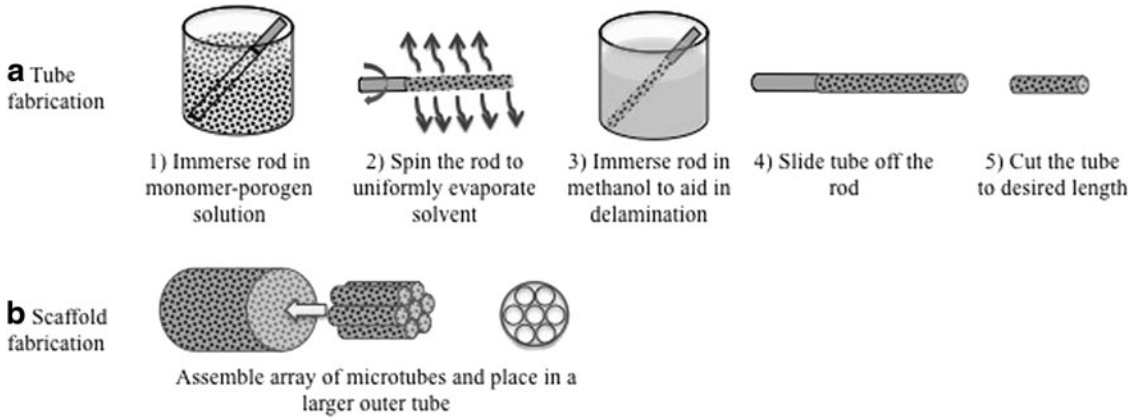

FIG. 1. Steps in fabricating PCL **(a)** tubes and **(b)** scaffolds. PCL, polycaprolactone.

surgical staples. Following surgery, rats were maintained in cages kept on heat pads (37°C) for 1 week and received banamine (1 mg/kg) and ampicillin (0.2 mg/kg) in Ringer's lactate for 3 days. Bladder care was performed twice daily at 12-h intervals for the first 2 weeks following surgery, and thereafter once daily until rats could urinate on their own, ~4 weeks after surgery.

Four weeks after implantation, rats with transected spinal cords were perfused with 4% paraformaldehyde (PFA; 4°C) and spinal cords were immersed in sucrose: PBS solution (30:70 weight ratio) for 48 h. Longitudinal sections (20 μm-thick) were obtained through cryosectioning. Slides were placed in proteinase K:antigen retrieval (1:20; Millipore, Darmstadt, Germany) for 20 min, washed in 50% methanol for 5 min, 100% methanol for 20 min, and again 50% methanol for 5 min, and were blocked with 5% goat serum in Tris-buffered saline (TBS) for 1 h. Axons were identified by Mouse Anti-Neurofilament 200 (1:500) (Millipore). Sections were washed with TBS. Slides were subsequently labeled with goat anti-mouse 488 (1:250; Life Technologies) as a secondary antibody for 1 h and washed with TBS. Sections were sealed with Flouromount G. Fluorescent images were taken and quantification analysis was performed using ImageJ software. Of $n=2$ of the animals which received implants, 1 μm-thick slides were cryosectioned, stained with Toluidine Blue, sputter coated with gold, and analyzed using electron microscopy.

Results

NaCl porogen size reduction

PMB was used to reduce the NaCl porogen particle size. After PBM at 100 rpm, regardless of time ranging from 1 to 90 min, a negligible reduction in the NaCl particle size was observed. It was likely that the kinetic energy was not sufficient to fracture particles.[11,24] To improve the kinetic energy, a maximal rotation speed of 400 rpm was used to correlate PBM time with NaCl particle size. To determine the particle size and characterize the surface morphology, SEM was conducted. The as-received NaCl consisted of particles with relatively smooth surfaces and an average diameter of 360 ± 115 μm (Fig. 2a). The NaCl particle size was reduced to 191 ± 70 μm with 1 min of PMB at 400 rpm (Fig. 2b). After 5 and 30 min of PMB at 400 rpm, the particle size was reduced to 43 ± 12 μm and 17 ± 10 μm, respectively (Fig. 2c, d). Compared with the as-received NaCl, the PBM particle surfaces and geometries were irregular, which is common when using a mechanical comminution process.[11,34,37] No significant change in particle size was observed after PMB at 400 rpm for more than 30 min, indicating that increasing time would not further significantly reduce particle size.

In mechanical comminution, it is common for the particle size to approach an asymptotic limit governed by the kinetic energy of a particular process.[11,35] Assuming the kinetic energy of each ball collision is fixed (by the rotational speed of the PBM in this case), it is known that the impact energy required to fracture particles is inversely proportional to the square root of the diameter of the particles. Thus, when the NaCl particles reached ~17 μm (at 400 rpm), increasing the PBM time did not further reduce the particle size. Nevertheless, the goal of this activity was to produce NaCl particles that were smaller (2–4×) than the scaffold walls (aimed to be 30–60 μm) to prevent line-of-site gaps between microchannels that would allow axons to lose longitudinal directionality as they extend toward distal targets. Thus, 17 μm diameter NaCl particles were sufficiently small to produce PCL tubes for scaffold fabrication.

Hierarchically ordered porosity in PCL

The fracture surface of a 100% solvent cast PCL exhibited no porosity (Fig. 3a), which was in agreement with previous reports.[24,26,35,37] As described in the previous section, 17 μm NaCl was selected as the porogen size to introduce porosity in PCL. The volume fraction of 17 μm NaCl porogen was varied between 0 and 70 vol % to form PCL films. Above 70 vol % NaCl, the samples were fragile and difficult to handle and thus not characterized. SEM was used to assess the pore morphology and distribution. Because one of the goals of this work was to reduce the PCL elastic modulus, the highest vol

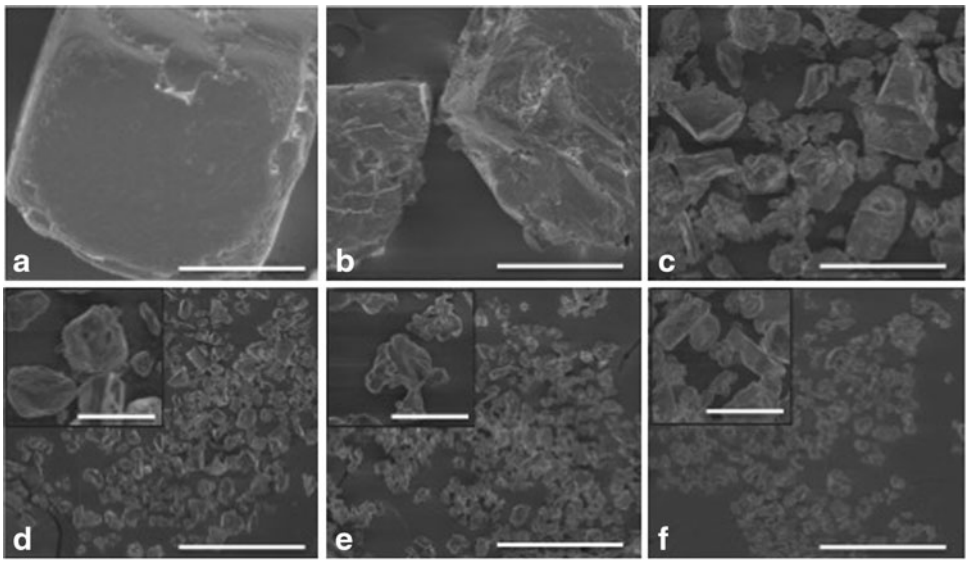

FIG. 2. Increasing the planetary ball-milling time reduces the particle size and size distribution. SEM images of NaCl **(a)** as-received, and NaCl ball-milled at 400 rpm for: **(b)** 1 min, **(c)** 5 min, **(d)** 30 min, **(e)** 60 min, and **(f)** 90 min. The *inset* scale bars are 25 μm; all other scale bars are 200 μm. rpm, Revolutions per minute; SEM, scanning electron microscopy.

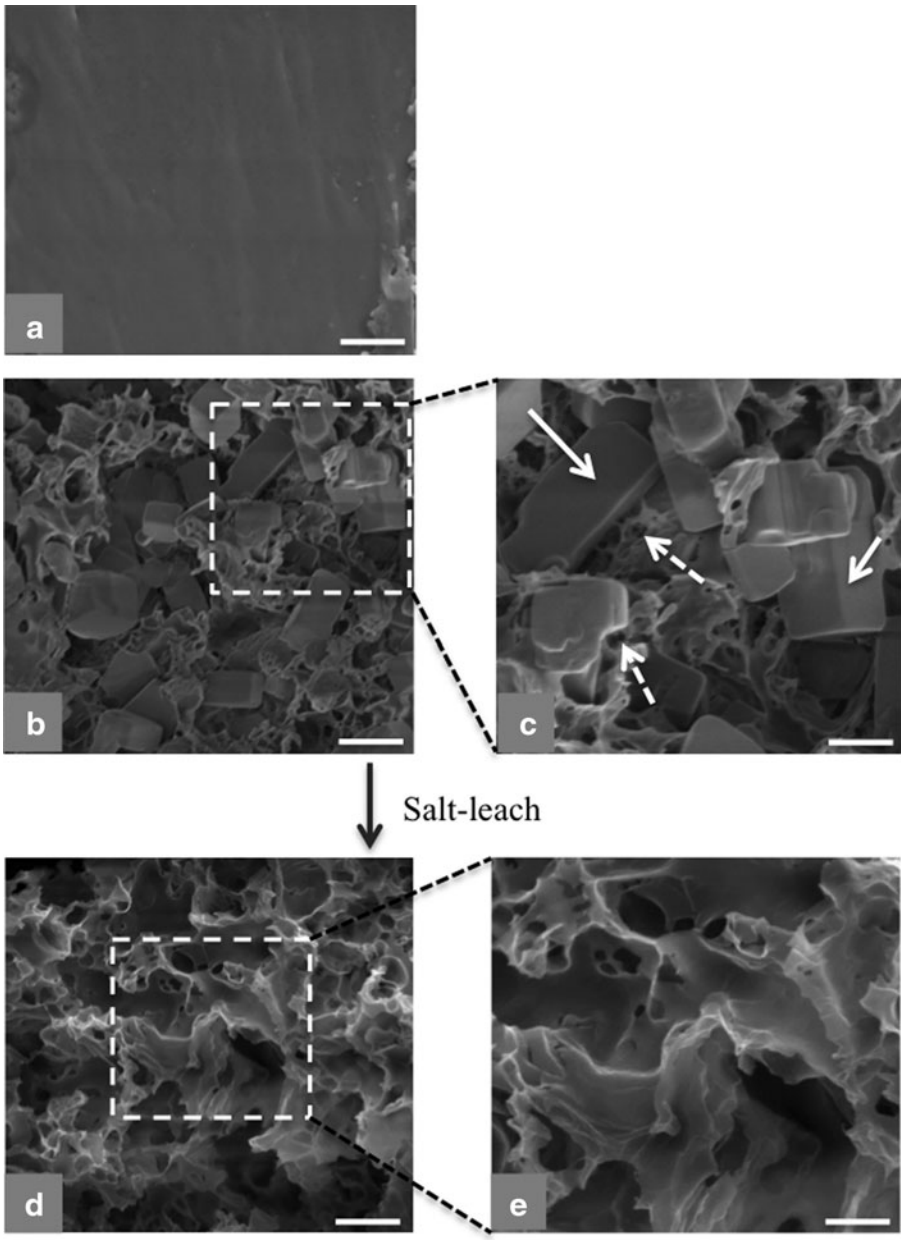

FIG. 3. Cross-sectional SEM analysis of PCL films. **(a)** One hundred percent PCL (no porosity). A 70 vol % porosity PCL film fabricated using 17 μm (average diameter) NaCl particles **(b)** before and **(d)** after salt-leaching. **(c, e)** 2× Magnification images of the *dashed boxes* shown in **(b, d)**, respectively. The *solid arrows* in **(c)** point to NaCl particles and the *dashed arrows* point to intrinsic porosities created in addition to porosities created by the porogen. Scale bars: **(a)** 2.5 μm, **(b, d)** 10 μm, and **(c, e)** 5 μm. vol %, Volume percent.

% porosity achieved (70%) was the focus and, therefore, this composition is used hereafter. SEM analysis was conducted on PCL before and after removal of the 17 μm NaCl porogen (NaCl ball-milled at 400 rpm for 60 min) (Fig. 3). Before salt-leaching, the NaCl particles (Fig. 3b, c) consisted of cuboidal or faceted NaCl particles embedded in PCL. After salt-leaching and removal of NaCl, pores with sizes similar to the NaCl particles were generated (Fig. 3d, e).

Additional observations were made. First, the cuboidal or faceted NaCl particles in Figure 3b and c did not resemble the irregular NaCl particle surfaces observed after 60 min of PBM at 400 rpm (Fig. 2e). It is possible that the NaCl/PCL monomer solution partially etched the NaCl particles resulting in a change in morphology from irregular before casting to cuboidal after casting. To investigate this, NaCl particles were exposed to chloroform and/or methanol with no PCL monomer present. The NaCl particles maintained their irregular shape in both cases (data not shown). Thus, the presence of PCL monomer is believed to cause partial etching resulting in smooth and faceted surfaces; however, further work is required to better understand this phenomenon. Second, in addition to the porosity created by the NaCl particles, a second smaller scale of porosity was observed. Because the smaller pores were apparent before salt-leaching, they are considered intrinsic; to be distinguished from the porosity created by salt-leaching. Overall, hierarchical porosity was generated: $\sim$17 μm pores were created by salt-leaching, whereas relatively smaller intrinsic pores were formed as a byproduct of the modified salt-leaching process. In addition, the total porosity increased the vol % porosity, which was predicted to reduce the elastic modulus and perhaps enhance cell attachment (discussed in Correlating Porosity with Mechanical Properties section and Cell Adhesion section).

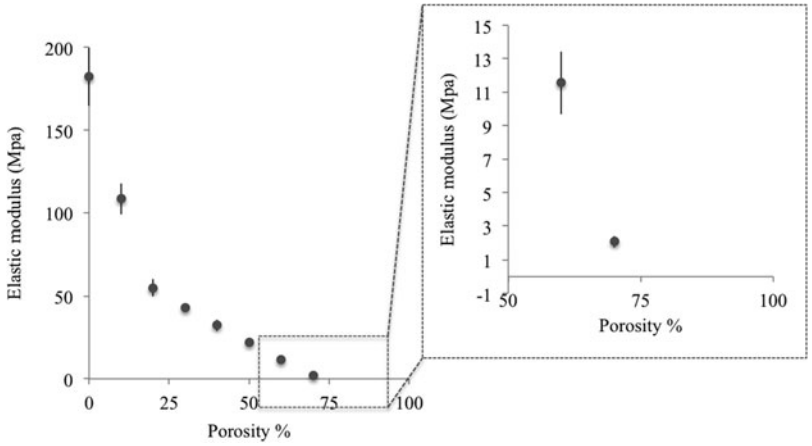

FIG. 4. The elastic modulus of PCL versus porosity percentage created by 17 μm NaCl particles.

Correlating porosity with mechanical properties

Since one of our goals was to reduce the stiffness of PCL, porosity was introduced using NaCl as a porogen. Tensile testing was used to measure the elastic modulus of PCL. To characterize the change in the elastic modulus as a function of porosity, PCL films with different porosities were used for tensile testing. The elastic moduli of PCL films decreased from 182.1 to 2.09 MPa when the porosity was increased from 0 to 70 vol % (Fig. 4) demonstrating the ability to control the stiffness of PCL by introducing porosity. Eshraghi and Das reported an average elastic modulus of 354.1 MPa for 100% solvent-cast PCL.[29] However, the study used a higher PCL MW, which likely explains the higher elastic modulus exhibited by the 100% PCL. Some other groups[12–14,35] generated porosity using a porogen (20–500 μm porogen sizes) and correlated the compressive modulus of PCL to porosity—the reported modulus of 80 vol % porous PCL is comparable to the present study. The modified salt-leaching process described herein introduced sufficient porosity to reduce the elastic modulus by nearly two orders of magnitude.

Cell adhesion

NIH 3T3 fibroblast cells did not adhere to uncoated nonporous PCL (Fig. 5d), but adhered to uncoated porous PCL (Fig. 5e). It is, therefore, shown that optimizing the porosity of PCL enhanced fibroblast cell adhesion. Similarly, when we coated PCL with fibronectin, regardless of its porosity and physical properties, NIH fibroblast cell attachment was observed (Fig. 5g, h). In contrast, primary Schwann cells did not adhere to uncoated porous PCL regardless of porosity (Fig. 5j, k). However, if PCL was coated with fibronection, Schwann cells adhered regardless of porosity (Fig. 5m, n). Thus, the adhesion ability to porous PCL is cell-specific and requires adhesion properties that are not ubiquitous among cell types.

Scaffold characterization

The scaffolds consisted of close-packed arrays of 70 vol % porosity microtubes in which inner channels were fabricated separately and inserted into a larger outer tube with similar porosity. In addition to the open space available by the inner microtubes, the unique scaffold architecture created interstitial cavities between tubes, which increased the total scaffold open volume. Both the inner and outer tubes consisted of 70 vol % porous salt-leached PCL. This composition was selected because it had interconnected porosity and the lowest elastic modulus while maintaining mechanical integrity for scaffold fabrication.

A representative cross-sectional image of a 2 mm-long PCL scaffold is shown in Figure 6a. The inner tubes of the scaffold had a wall thickness of 60 ± 15 μm and an average ID of 260 μm. The outer tube ID was 1.62 mm (1620 μm) with a wall thickness of 90 μm occupying an outer diameter (OD) of 1.80 mm (1800 μm). The ID of the inner tubes was selected as 200–300 μm since linear axon growth was previously demonstrated in microchannel scaffolds with 200 μm-diameter channels[15,17,19,25] while our unpublished data indicated that axons lose directionality when channels are larger than 300 μm. In addition, the PCL scaffold was designed to have an OD of 1.8 mm to fit in the T3 rat spinal column, which has an average diameter of 1.8 mm.

SEM images of the inner surface, cross-section, and outer surface of the inner PCL tubes confirmed interconnected porosity with average pore size of 17 μm (the cross-sectional image is shown in Fig. 6b). The scale of the porosity is believed to be sufficiently small to prevent axonal growth orthogonal to the microtubes. Few studies successfully fabricated microchannel scaffolds with the described wall porosity; nevertheless, the scaffolds had <45% open volume.[15,16,18–20,25,27,38] In addition, since the NaCl particles used during scaffold fabrication were 17 μm in diameter, tubes with a wall thickness of about 20 μm can be made. Therefore, fabricating microtubes with a wall thickness of 20 μm using this scaffold fabrication technique can produce scaffolds with over 85% open volume, which would be a significant improvement compared with previously described nerve guidance scaffolds.

Characterization of porous PCL scaffolds in vivo

Animals receiving sham surgeries were not paralyzed after the procedure and therefore histology analysis was not performed. Typical histological images of the spinal cord can be found in literature for comparison.[39,40] Since the most promising cell attachment results were obtained with fibronectin-coated porous PCL, the same material and coating combination was translated into scaffolds for *in vivo* studies. Experimental groups included animals with T3 transected spinal cords (1.2 mm long) without implants ($n = 3$) or animals

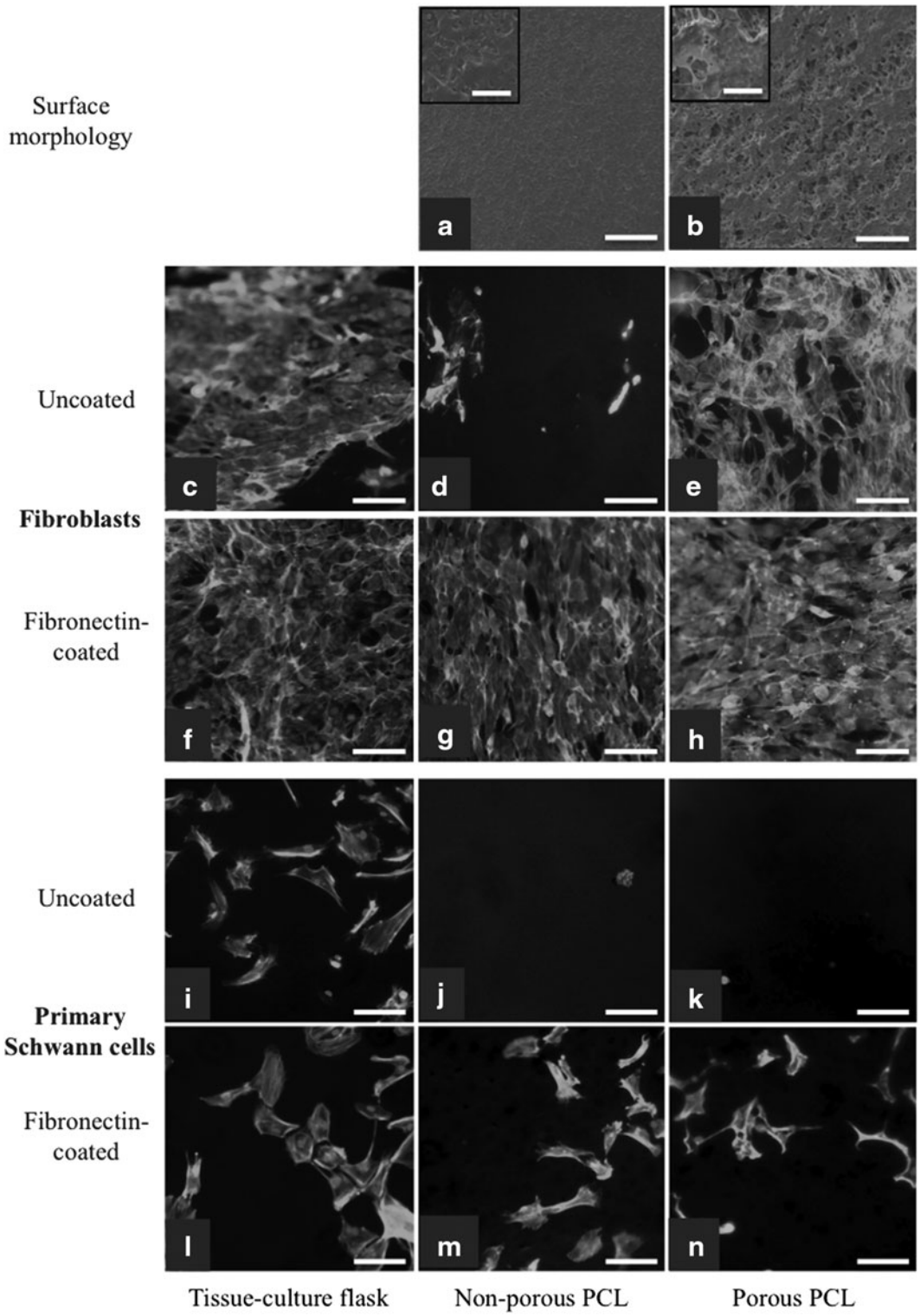

FIG. 5. Fibroblast and primary rat Schwann cell attachment on PCL films. SEM images of the *top* surface of **(a)** nonporous PCL film and **(b)** 70 vol % porosity PCL with corresponding magnified images demonstrate an increased surface roughness in porous PCL. NIH 3T3 fibroblasts were cultured on uncoated **(c)** tissue-culture treated flask as control, **(d)** nonporous PCL film and **(e)** 70 vol % porosity PCL film, and on fibronectin-coated **(f)** tissue culture-treated flask, **(g)** nonporous PCL film, and **(h)** 70 vol % porosity PCL film. Cells were fixed after 72 h and stained for actin and nuclei. Unlike nonporous PCL, 70 vol % porosity PCL films provided cell attachment comparable to the positive control. Both groups exhibited cell attachment after fibronectin coating. Similarly, primary rat Schwann cells were cultured on uncoated **(i)** PDL surfaces as control, **(j)** nonporous PCL, and **(k)** 70 vol % porosity PCL as well as fibronectin-coated **(l)** PDL surfaces, **(m)** nonporous PCL, and **(n)** 70 vol % porous PCL films. Cells were fixed and stained for actin in *green* and nuclei in *blue* 72 h postseeding. While Schwann cells did not attach to uncoated PCL films with or without porosity, cell attachment occurred on both fibronectin-coated PCL surfaces. Scale bars in the *insets* in **(a, b)** are 10 μm. All other scale bars are 100 μm.

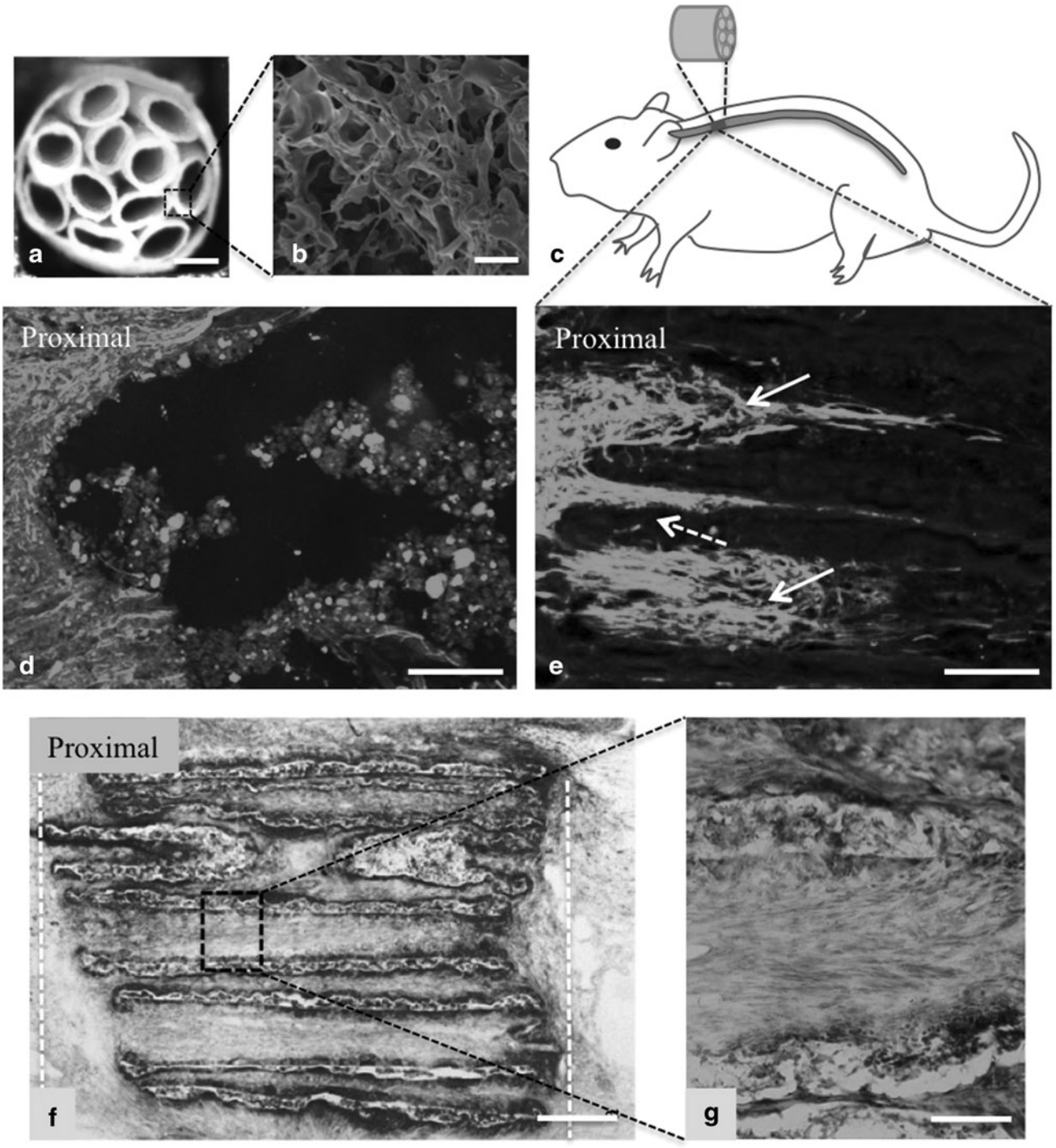

FIG. 6. PCL scaffold characterization and *in vivo* studies. **(a)** Cross-sectional image of a PCL scaffold with inner tubes of 260 μm in diameter, fabricated from 70 vol % porosity PCL. SEM image of an inner tube cross-section is shown in **(b)**, which shows interconnected porosity. **(c)** A schematic of fibronectin-coated porous PCL scaffold is shown, which was inserted in the transected T3 section of a rat spinal cord. Four weeks post-implantation, animals were perfused and longitudinal sections were obtained and stained with neurofilament (NF200). **(d)** Transected spinal cord without an implant showed minimum axon penetration into the lesion. **(e)** The proximal site of the scaffold shows linear axon growth into PCL scaffolds. *Solid white arrows* in **(e)** demonstrate the axons grew linearly inside the microtubes, whereas the *dashed arrow* indicates some axons grew linearly in between the microtubes. **(f)** Toluidine Blue staining of PCL scaffold 4 weeks postimplantation shows that the scaffold microtubes were maintained and minimum scar tissue formation was observed around the scaffold. The *white dashed lines* show the boundary of the implanted scaffold in the transected spinal cord. The *boxed* region in **(f)** is magnified in **(g)**, which highlights the intimate contact of cells with scaffold walls. Scale bars: **(a)** 300 μm, **(b)** 100 μm, **(d, e)** 200 μm, **(f)** 250 μm, and **(g)** 50 μm.

with T3 transected spinal cords (2 mm-long) receiving fibronectin-coated 70 vol % porosity PCL scaffolds ($n = 8$) (Fig. 6c). After 4 weeks, spinal cord tissue was analyzed by histology. Longitudinal sections of spinal cords of all the animals without implants and $n = 6$ of the animals with PCL scaffolds were sliced and immunostained for neurofilament 200. Animals with transected spinal cords, but no implants, exhibited minimum axonal penetration into the lesion (Fig. 6d). However, neurofilament-labeled axons grew into the scaffold channels and extended linearly through the scaffolds for distances up to 0.5 mm (Fig. 6e).

Axon counting indicated over 70% increase in the number of axons that were observed 0.5 mm into the lesion for subjects that received PCL scaffolds compared with no implants. In addition, Toluidine Blue staining, ($n = 2$) showed that the scaffolds were present after 4 weeks *in vivo* and had not yet degraded (Fig. 6f). Minimum reactive cell layer is observed around the scaffold and axons are in close proximity to the scaffold walls (Fig. 6f, g), which is an indication of the promising biocompatibility response of the scaffolds to the nerve tissue.

Discussion

Microchannel scaffolds are a promising approach to linearly guide growing axons through injured spinal cord.[15–20] However, existing scaffold technologies require further refinement to establish clinical translation. Particularly, current microchannel scaffolds have often produced scaffolds with <45% open volume, which significantly reduces the therapeutic application of the scaffolds. In addition, a reactive cell layer is often formed at the distal end of the scaffold, which blocks the penetration of regenerated axons into the host tissue.[15,17] To address these two barriers, we investigated advanced materials processing and novel scaffold fabrication approaches to develop nerve guidance scaffolds exhibiting an unprecedented combination of features that improved the scaffold design, whereas reduced the scar tissue formation at the distal end of the scaffold. It is predicted that, in the presence of growth factors and/or engrafted Schwann cells or stem cells, the axon growth rate and density will be increased and the present scaffold technology becomes a viable approach for investigating spinal cord repair.

To improve the design of microchannel scaffolds, we focused on increasing scaffold open volume compared with state-of-the-art technology. Herein, a process was developed to fabricate scaffolds with a unique architecture to enable high open volume. Rather than fabricate arrays of microchannels in one step, this process entails the fabrication of individual thin wall tubes that were assembled into close-packed arrays (Fig. 1). This fabrication approach created additional interstitial volume between the microtubes that is equally capable of linearly guiding axons toward distal targets. Second, the novel scaffold manufacturing process provided the impetus to develop alternative materials to enable the fabrication of individual, thin-walled tubes. Hydrogels in general, do not exhibit adequate mechanical properties and are not compatible with this process. Hence, PCL was selected owing to its higher stiffness and strength. In its dense form, however, PCL was too stiff and brittle during implantation. We hypothesized that introducing porosity into PCL reduces the stiffness, thus improving its biocompatibility.

Several techniques have been previously studied to introduce porosity. Since the goal of this work was to increase scaffold open volume by reducing the scaffold wall thickness to ≤60 μm, the pore size had to be well below 60 μm to prevent axon crossover between microchannels. To fabricate PCL with micron to a few tens of micrometer diameter porosity, controlling the pore size and pore size distribution were necessary. Few techniques have been developed to create and control porosity in PCL. For example, techniques such as photo crosslinking of a modified PCL[27,34,37] and a customized patterning technique[7] were developed to pattern porous PCL nerve guidance scaffolds. However, in these studies, the porosity was >450 μm in diameter, which is significantly above our targeted porosity. Selective laser sintering is also a patterning technology used to create pores in PCL.[29,32,33,36] Although the pore size distribution was precisely controlled, the pores were >30 μm, which may potentially allow the axons to grow between scaffold walls and lose directionality along the lesion cavity as mentioned above.

Solvent casting is another technique to fabricate porous PCL by mixing a porogen with the monomer solution or melted polymer, forming a solid polymer and selectively etching the porogen with a solvent. Porogens, such as polypropylene glycol,[23] polyethylene glycol (PEG),[24] sodium chloride (NaCl),[34,37] and a mixture of PEG and NaCl[35] were used to create pores within PCL. Although there are examples that demonstrate the ability to create interconnected porosity,[24,35,37] control of pore size and pore size distribution can be difficult. Moreover, the diameter of the NaCl porogen particles that have been previously characterized are generally >150 μm in diameter.[34] When the porogen size was reduced by intensive mixing, the distribution of the particle size was relatively large (from 20 to 500 μm).[35] In another study, the pore size of a PCL conduit generated by NaCl porogen ground with mortar and pestle was reduced to 10–38 μm and allowed the permeation of soluble factors.[37] Overall, to our knowledge, the present study is the first report that controls pore size in PCL through salt-leaching while generating interconnected porosity.

Through tensile testing, it was determined that the elastic modulus of PCL films reduced by over 86% when a 70 vol % porosity was introduced. In addition, compared with porous and dense PCL, we believed that the surface roughness of porous PCL could increase cell adhesion (Fig. 5a, b). In addition, previous reports have used chemical modifications to enhance cell attachment.[15–20,26,28,33,38] For example, a composition of PCL and proteins such as collagen and hyaluronic acid (HA) improved cell attachment.[22,23,33,38] Thus, cell attachment studies involved dense versus porous PCL, with and without fibronectin coating, using fibroblasts and Schwann cells as example cell lines to study the cell adhesion properties of the material (Fig. 5). Herein, we show that depending on the cell type and protein coating, porous PCL could improve cell adhesion properties (Fig. 5) likely due to an increase in surface roughness and wettability of PCL.

Upon *in vitro* analysis, microchannel scaffolds consisting 60% open volume were fabricated from porous and fibronectin-coated PCL and tested *in vivo*. After 4 weeks of *in vivo* testing, the microtube PCL scaffolds maintained integrity and demonstrated the ability to linearly guide axons. Although no intervention was done in this study to promote axon density and, therefore, the number of axons that were

present in the scaffold was not statistically significant or clinically viable, the scaffolds are considered effective for guiding growing axons along the longitudinal axis of the spinal cord. Moreover, axons did not cross through the scaffold walls as shown in Figure 6f and grew both inside and between the inner tubes demonstrating that the entire open volume of the scaffold (including the space between the inner tubes) is effectively available for linear nerve growth. While minimum scar tissue formation around the scaffolds were observed, additional inflammatory response assays as well as the long-term biocompatibility and degradation analysis of the scaffolds are necessary to make conclusions on the biocompatibility of the scaffolds. In addition, in our follow-up work, the described scaffold fabrication technique will be translated to faster degrading materials such as poly (lactic-co-glycolic acid) (PLGA).

Conclusion

The pore size and pore size distribution of PCL is controlled by using a modified salt-leaching technique and optimizing the porogen size and distribution using PMB. By increasing the volume fraction of porosity, the elastic modulus of PCL was reduced from 182.1 to 2.09 MPa. In addition, the cell adhesion on PCL was improved by increasing porosity and/or fibronectin coating. To create spinal cord nerve guidance scaffolds, porous PCL microchannel scaffolds were fabricated consisting of 60 μm wall thickness, 260 μm ID microtubes, and 60% open volume (compared with <45% open volume state-of-the-art scaffolds). In addition, the scaffold length could be increased from mm-scale to clinically relevant cm-scale.

The scaffold *in vivo* performance was studied in a rat T3 full-transection spinal cord model. Linear growth of axons was observed through both the microtubes interior as well as in the interstitial space in between the microtubes, demonstrating that the entire 60% open volume of the scaffold can effectively be used for nerve growth and linear guidance. Also the scaffold was not degraded after 4 weeks, which is beneficial for clinically relevant cm-long nerve gaps that require slower degradation rates. In addition, minimum scar tissue formation was observed around the scaffold, which indicated favorable biocompatibility with the nerve tissue. Overall, this work presents a modified salt-leaching process combined with a novel scaffold preparation technique to fabricate high open volume nerve guidance scaffolds for spinal cord repair.

Acknowledgments

The authors thank their sponsors, the NIH (R01 EB014986), the Veterans Administration, and the Dr. Miriam and Sheldon G. Adelson Medical Research Foundation. The National Science Foundation is also greatly appreciated for a Graduate Research Fellowship to D.S.

Disclosure Statement

No competing financial interests exist.

References

1. Silva, N.A., Sousa, N., Reis, R.L., and Salgado, A.J. From basics to clinical: a comprehensive review on spinal cord injury. Prog Neurobiol **114,** 25, 2014.
2. Varma, A.K., Das, A., Wallace, G., IV, Barry, J., Vertegel, A.A., Ray, S.K., and Banik, N.L. 2013. Spinal cord injury: a review of current therapy, future treatments, and basic science frontiers. Neurochem Res **38,** 895, 2013.
3. Mahoney, M.J., and Anseth, K.S. Three-dimensional growth and function of neural tissue in degradable polyethylene glycol hydrogels. Biomaterials **27,** 2265, 2006.
4. Xu, X.M., Guénard, V., Kleitman, N., and Bunge, M.B. Axonal regeneration into Schwann cell-seeded guidance channels grafted into transected adult rat spinal cord. J Comp Neurol **351,** 145, 1995.
5. McDonald, J.W., Liu, X.Z., Qu, Y., Liu, S., Mickey, S.K., Turetsky, D., Gottlieb, D.I., and Choi, D.W. Transplanted embryonic stem cells survive, differentiate and promote recovery in injured rat spinal cord. Nat Med **5,** 1410, 1999.
6. Lu, P., Jones, L.L., Snyder, E.Y., and Tuszynski, M.H. Neural stem cells constitutively secrete neurotrophic factors and promote extensive host axonal growth after spinal cord injury. Exp Neurol **181,** 115, 2003.
7. Shor, L., Güçeri, S., Wen, X., Gandhi, M., and Sun, W. Fabrication of three-dimensional polycaprolactone/hydroxyapatite tissue scaffolds and osteoblast-scaffold interactions in vitro. Biomaterials **28,** 5291, 2007.
8. Wang, X., Hu, W., Cao, Y., Yao, J., Wu, J., and Gu, X. Dog sciatic nerve regeneration across a 30-mm defect bridged by a chitosan/PGA artificial nerve graft. Brain **128,** 1897, 2005.
9. Chow, W.N., Simpson, D.G., Bigbee, J.W., and Colello, R.J. Evaluating neuronal and glial growth on electrospun polarized matrices: bridging the gap in percussive spinal cord injuries. Neuron Glia Biol **3,** 119, 2007.
10. Meiners, S., Ahmed, I., Ponery, A.S., Amor, N., Harris, S.L., Ayres, V., Fan, Y., Chen, Q., Delgado-Rivera, R., and Babu, A.N. Engineering electrospun nanofibrillar surfaces for spinal cord repair: a discussion. Polym Int **56,** 1340, 2007.
11. German, R.M. Powder Metallurgy Science. Princeton, NJ: Metal Powder Industry, 1984.
12. Woerly, S., Doan, V.D., Evans-Martin, F., Paramore, C.G., and Peduzzi, J.D. Spinal cord reconstruction using NeuroGel™ implants and functional recovery after chronic injury. J Neurosci Res **66,** 1187, 2001.
13. Wen, X., and Tresco, P.A. Fabrication and characterization of permeable degradable poly (DL-lactide-co-glycolide) (PLGA) hollow fiber phase inversion membranes for use as nerve tract guidance channels. Biomaterials **27,** 3800, 2006.
14. Whittlesey, K.J., and Shea, L.D. Nerve growth factor expression by PLG-mediated lipofection. Biomaterials **27,** 2477, 2006.
15. Stokols, S., Sakamoto, J., Breckon, C., Holt, T., Weiss, J., and Tuszynski, M.H. Templated agarose scaffolds support linear axonal regeneration. Tissue Eng **12,** 2777, 2006.
16. Prang, P., Müller, R., Eljaouhari, A., Heckmann, K., Kunz, W., Weber, T., Faber, C., Vroemen, M., Bogdahn, U., and Weidner, N. The promotion of oriented axonal regrowth in the injured spinal cord by alginate-based anisotropic capillary hydrogels. Biomaterials **27,** 3560, 2006.
17. Gros, T., Sakamoto, J.S., Blesch, A., Havton, L.A., and Tuszynski, M.H. Regeneration of long-tract axons through sites of spinal cord injury using templated agarose scaffolds. Biomaterials **31,** 6719, 2010.
18. Tuinstra, H.M., Aviles, M.O., Shin, S., Holland, S.J., Zelivyanskaya, M.L., Fast, A.G., Ko, S.Y., Margul, D.J.,

Bartels, A.K., Boehler, R.M., and Cummings, B.J. Multifunctional, multichannel bridges that deliver neurotrophin encoding lentivirus for regeneration following spinal cord injury. Biomaterials **33,** 1618, 2012.
19. Gao, M., Lu, P., Bednark, B., Lynam, D., Conner, J.M., Sakamoto, J., and Tuszynski, M.H. Templated agarose scaffolds for the support of motor axon regeneration into sites of complete spinal cord transection. Biomaterials **34,** 1529, 2103.
20. Pawar, K., Cummings, B.J., Thomas, A., Shea, L.D., Levine, A., Pfaff, S., and Anderson, A.J. Biomaterial bridges enable regeneration and re-entry of corticospinal tract axons into the caudal spinal cord after SCI: association with recovery of forelimb function. Biomaterials **65,** 1, 2015.
21. Shahriari, D., Koffler, J., Lynam, D.A., Tuszynski, M.H., and Sakamoto, J.S. Characterizing the degradation of alginate hydrogel for use in multilumen scaffolds for spinal cord repair. J Biomed Mater Res A **104,** 611, 2016.
22. Dunnen, W.D., Robinson, P.H., Wessel, R.V., Pennings, A.J., Leeuwen, M.V., and Schakenraad, J.M. Long-term evaluation of degradation and foreign-body reaction of subcutaneously implanted poly (DL-lactide-e-caprolactone). J Biomed Mater Res **36,** 337, 1997.
23. Chiang, H.Y., Chien, H.F., Shen, H.H., Yang, J.D., Chen, Y.H., Chen, J.H., and Hsieh, S.T. Reinnervation of muscular targets by nerve regeneration through guidance conduits. J Neuropathol Exp Neurol **64,** 576, 2005.
24. Lin, W.J., and Lu, C.H. Characterization and permeation of microporous poly (ε-caprolactone) films. J Membr Sci **198,** 109, 2002.
25. Callister, W.D., and Rethwisch, D.G. Materials Science and Engineering: An Introduction, 8th ed. Hoboken, NJ: Wiley Global Education, 2009.
26. Santiago, L.Y., Nowak, R.W., Rubin, J.P., and Marra, K.G. Peptide-surface modification of poly (caprolactone) with laminin-derived sequences for adipose-derived stem cell applications. Biomaterials **27,** 2962, 2006.
27. Elomaa, L., Teixeira, S., Hakala, R., Korhonen, H., Grijpma, D.W., and Seppälä, J.V. Preparation of poly (ε-caprolactone)-based tissue engineering scaffolds by stereolithography. Acta Biomater **7,** 3850, 2011.
28. Prabhakaran, M.P., Venugopal, J., Chan, C.K., and Ramakrishna, S. Surface modified electrospun nanofibrous scaffolds for nerve tissue engineering. Nanotechnology **19,** 455102, 2008.
29. Eshraghi, S., and Das, S. Mechanical and microstructural properties of polycaprolactone scaffolds with one-dimensional, two-dimensional, and three-dimensional orthogonally oriented porous architectures produced by selective laser sintering. Acta Biomater **6,** 2467, 2010.
30. Tunturi, A.R. Elasticity of the spinal cord, pia, and denticulate ligament in the dog. J Neurosurg **48,** 975, 1978.
31. Ozawa, H., Matsumoto, T., Ohashi, T., Sato, M., and Kokubun, S. Comparison of spinal cord gray matter and white matter softness: measurement by pipette aspiration method. J Neurosurg **95,** 221, 2001.
32. Williams, J.M., Adewunmi, A., Schek, R.M., Flanagan, C.L., Krebsbach, P.H., Feinberg, S.E., Hollister, S.J., and Das, S. Bone tissue engineering using polycaprolactone scaffolds fabricated via selective laser sintering. Biomaterials **26,** 4817, 2005.
33. Wiria, F.E., Leong, K.F., Chua, C.K., and Liu, Y. Poly-ε-caprolactone/hydroxyapatite for tissue engineering scaffold fabrication via selective laser sintering. Acta Biomater **3,** 1, 2007.
34. Kweon, H., Yoo, M.K., Park, I.K., Kim, T.H., Lee, H.C., Lee, H.S., Oh, J.S., Akaike, T., and Cho, C.S. A novel degradable polycaprolactone networks for tissue engineering. Biomaterials **24,** 801, 2003.
35. Reignier, J., and Huneault, M.A. Preparation of interconnected poly (ε-caprolactone) porous scaffolds by a combination of polymer and salt particulate leaching. Polymer **47,** 4703, 2006.
36. Yeong, W.Y., Sudarmadji, N., Yu, H.Y., Chua, C.K., Leong, K.F., Venkatraman, S.S., Boey, Y.C.F., and Tan, L.P. Porous polycaprolactone scaffold for cardiac tissue engineering fabricated by selective laser sintering. Acta Biomater **6,** 2028, 2010.
37. Kokai, L.E., Lin, Y.C., Oyster, N.M., and Marra, K.G. Diffusion of soluble factors through degradable polymer nerve guides: controlling manufacturing parameters. Acta Biomater **5,** 2540, 2009.
38. Schnell, E., Klinkhammer, K., Balzer, S., Brook, G., Klee, D., Dalton, P., and Mey, J. Guidance of glial cell migration and axonal growth on electrospun nanofibers of poly-ε-caprolactone and a collagen/poly-ε-caprolactone blend. Biomaterials **28,** 3012, 2007.
39. Weirich, S.D., Cotler, H.B., Narayana, P.A., Hazle, J.D., Jackson, E.F., Coupe, K.J., Mcdonald, C.L., Langford, L.A., and Harris, J.H., Jr. Histopathologic correlation of magnetic resonance imaging signal patterns in a spinal cord injury model. Spine **15,** 630, 1990.
40. Ma, M., Basso, D.M., Walters, P., Stokes, B.T., and Jakeman, L.B. Behavioral and histological outcomes following graded spinal cord contusion injury in the C57Bl/6 mouse. Exp Neurol **169,** 239, 2001.

Address correspondence to:
Jeff S. Sakamoto, PhD
Department of Mechanical Engineering
University of Michigan
Ann Arbor, MI 48109

E-mail: jeffsaka@umich.edu

Received: September 16, 2016
Accepted: January 11, 2017
Online Publication Date: March 31, 2017